Strain-induced magnetic anisotropies in Co films on Mo(110)

J. Prokop, D. A. Valdaitsev, A. Kukunin, M. Pratzer, G. Schönhense, and H. J. Elmers
Institut für Physik, Johannes Gutenberg-Universität Mainz, Staudingerweg 7, D-55099 Mainz, Germany
(Received 28 November 2003; revised manuscript received 5 August 2004; published 16 November 2004)

Mo/Co(0001)/Mo(110) epitaxial films were grown by molecular beam epitaxy in ultrahigh vacuum on $(11\bar{2}0)$ oriented α-Al_2O_3 substrates. Co grows on Mo(110) in the Nishiyama-Wassermann orientation, i.e., $[1\bar{1}00]$Co$\|[1\bar{1}0]$Mo. Low energy electron diffraction reveals a lateral expansive strain of the Co film independent of the thickness. Magnetic anisotropies were obtained from hard-axis magnetization loops measured by Kerr magnetometry in longitudinal and polar geometry. Magnetic interface anisotropies are very small (<0.04 mJ/m^2). Deviations of the volume-type in-plane ($K_{v,p}=0.79$ MJ/m^3) and out-of-plane ($K_v=-9.5$ MJ/m^3) anisotropies from bulk values for hexagonal-close-packed Co are attributed to magnetoelastic anisotropies.

DOI: 10.1103/PhysRevB.70.184423 PACS number(s): 75.30.Gw, 75.70.Ak, 78.20.Ls

I. INTRODUCTION

The origin of magnetic anisotropies is a topic of current interest. The relation between magnetic anisotropies and the anisotropy of the orbital moment[1] was confirmed by recent experimental investigations.[2–4] Both anisotropies are induced by the spin-orbit coupling that nowadays can be routinely considered in theoretical approaches leading to an understanding of this phenomenon beyond the phenomenological description.[5,6] The high symmetry of bulk materials usually quenches orbital moments and magnetic anisotropies to a large extent. This is no longer true for magnetic anisotropies that are induced by the interaction of ultrathin films with the substrate. In addition to the shape anisotropy two types of anisotropies dominate the magnetic anisotropies of ultrathin films: Néel-type[7] magnetic interface anisotropy originating from the symmetry breaking spin-orbit coupling at the interface and magnetoelastic anisotropy resulting from the epitaxial strain.[8,9]

The body-centered-cubic (bcc)(110) surfaces of W and Mo are very suitable substrates for growing magnetic thin films, as their free surface enthalpy is high and interdiffusion or surface alloying generally do not occur. Both metals can be classified as early transition metals with similar chemical properties and moreover they have almost the same lattice constants. Contrarily, the magnetic anisotropies for Fe/Mo(110) and Fe/W(110) films behave completely different. While the magnetic easy axis is directed along $[1\bar{1}0]$ for ultrathin Fe/W(110) films,[10] the magnetic anisotropy prefers the [001] easy axis for Fe/Mo(110) films.[11] This difference was attributed to the Néel type interface anisotropy.[11] Magnetic anisotropies for Co/W(110) favor the $[1\bar{1}0]$ easy axis,[12] similar to the case of Fe/W(110). For the case of Co/W(110), the contribution of magnetoelastic anisotropies could be isolated, and were explained by bulk magnetostriction properties.[12] However, the validity of bulk magnetostriction properties for ultrathin films is questionable.[13–16] Direct measurements of the magnetoelastic coupling coefficients using the bending cantilever technique,[14] revealed that magnetoelastic coefficients strongly depend on the strain, and considerably deviate from bulk values for strain values of the order of a few percent.[14,15] Large strain values of this size are typical for thin epitaxial metallic films. Moreover, in order to get a full picture of the thin films magnetic anisotropies, the role of thermal excitations in magnetic anisotropy has to be considered.[15,17] For Co films, a discussion of magnetic anisotropies may be even more complicated due to possible stacking faults in hcp layer stacks, as shown for Co/W(001).[18,19]

The present paper concerns magnetic anisotropies in the Co/Mo(110) system. As we show, the comparison of W(110) and Mo(110) substrates provides an important insight into the role of strain induced and spin-orbit coupling induced magnetic anisotropies. We have examined the anisotropies in ultrathin Co/Mo(110) films using films of varying thickness. While the magnetic surface anisotropy (MSA) is proportional to the film area A, the volume type anisotropies increase like At, where t denotes the film thickness. In our phenomenological definition MSA then includes all anisotropy contributions which are proportional to A.

Contributions from the MSA can be separated from the volume-type anisotropies by plotting the total film anisotropy versus t and then to obtain the MSA from the axial section. The Néel-type interface anisotropy contributes exclusively to the MSA. The strain induced anisotropy may contribute to both MSA and volume-type anisotropy, because the epitaxial strain frequently relaxes following an approximate $1/t$ - law, at least in some range of thickness.[20,21] In thickness regimes with constant strain the magnetoelastic anisotropy contributes to the volume-type anisotropy, only, while in regimes of relaxing strain it appears as an MSA.

We present a measurement of the MSA of Co/Mo(110) using a wedge shaped sample of continuously varying thickness. The epitaxial strain for Co on Mo(110) is investigated in greater detail than previous measurements[22,23] and proves to be different to the Co/W(110) system. The uniaxial in-plane anisotropy is determined from hard-axis loops measured by Kerr magnetometry. The magnetization component along the external field could be isolated from the nonlinear Kerr contributions resulting from a mixing of longitudinal and transversal components,[24,25] using Kerr signals measured

 ©2004 The American Physical Society

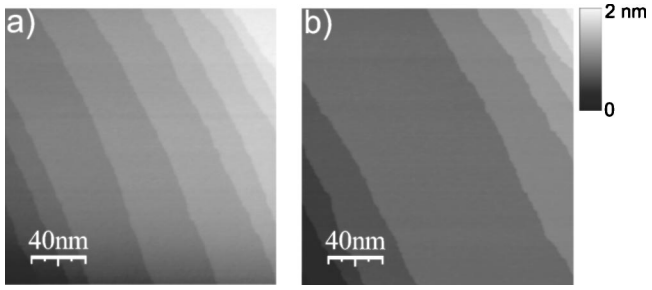

FIG. 1. 200×200 nm^2 STM images of the Mo(110) seed layer prepared on *a*-plane $(11\bar{2}0)$ α-Al_2O_3 substrate, taken at different places of the same sample. Terraces with widths between 10 and 50 nm are separated by steps of monoatomic height (a). One can also find broad terraces with the widths even up to 100 nm (b). The surface of the Mo films are qualitatively similar to a single crystal surface.

at two different polarization angles. We will show that the Néel-type MSA caused by the spin-orbit coupling at the interface is small (<0.04 mJ/m^2) and that in-plane volume anisotropies are likely caused by epitaxial strain. Bulk magnetostriction properties of Co do not explain quantitatively the observed magnetic anisotropies.

II. EXPERIMENT

The Mo(110) surface was prepared by the epitaxial growth of Mo on *a*-plane $(11\bar{2}0)$ α-Al_2O_3 substrates using ultrahigh vacuum electron-beam evaporation. A 250-nm-thick Mo seed layer was deposited at 1000 K. The deposition rate for the Mo seed layer was 0.5 nm/min as measured by a quartz monitor. Before the Co was deposited, the Mo film was cleaned by repeated cycles of flashing in 2×10^{-8} mbar oxygen atmosphere up to 1300 K, followed by flashing at 1800 K. The cleanness of the surface was checked by Auger electron spectroscopy. Structural measurements using low energy electron diffraction (LEED) reveals a Mo bcc(110) surface with the $[\bar{1}11]$ axis parallel to the $[\bar{1}100]$ direction of the Al_2O_3 substrate.[26–28] The prepared Mo surfaces are of the high quality. They are comparable to single crystal surfaces, as determined by scanning tunneling microscopy (STM)(see Fig. 1). The surface of the Mo seed layers reveals monoatomic terraces of the widths between 10 and 100 nm, and the steps density of the surface is similar to a single crystal surface.[29,30]

The Co films were deposited starting 2 min after the substrate was flashed. The substrate temperature was $\approx$600 K at the beginning of deposition at a constant growth rate of 0.5 nm/min and decreasing during the growth of thicker films. A wedge (0–10 nm) with a total length of 5 mm was prepared using a shadow mask. For *ex situ* measurements the films were protected against corrosion with a 3-nm-thick Mo capping, deposited at room temperature.

Magnetic properties were measured by analyzing the longitudinal Kerr rotation of *s*- and *sp*-polarized light of a 670 nm laserdiode, with the external field applied along the easy ($[\bar{1}10]$) and hard ([001]) axis in the film plane. The angle of incidence was adjusted to 45° with respect to the film normal. In addition we obtained data for the out-of-plane anisotropy from the Kerr rotation in polar geometry with the field applied perpendicular to the surface. In this case the angle of incidence was minimized ($<1°$).

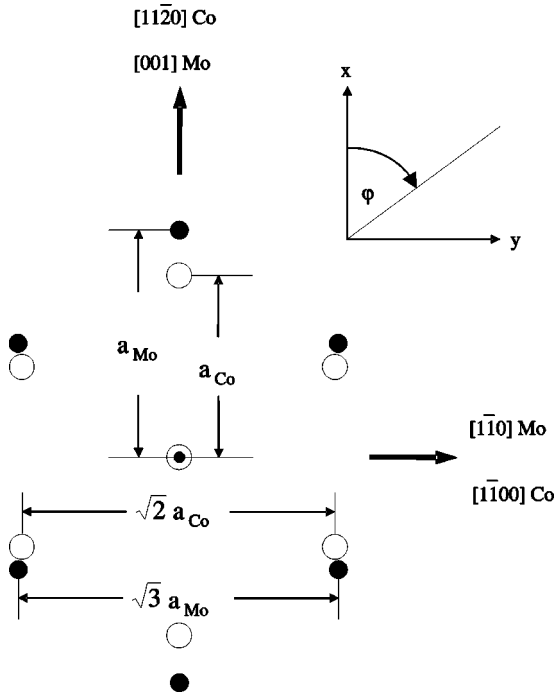

FIG. 2. Comparison of atomic positions in Mo(110) (solid circles) and Co(0001) (open circles). The figure shows positions in bulk lattice planes in Nishiyama-Wassermann orientation, i.e., $[\bar{1}100]$Co$\|[\bar{1}10]$Mo. The misfits of Co with respect to Mo in the *x* and *y* direction are given by $f_x=(a_{Co}-a_{Mo})/a_{Mo}=-0.203$ and $f_y=(\sqrt{3}a_{Co}-\sqrt{2}a_{Mo})/\sqrt{2}a_{Mo}=-0.024$.

III. GROWTH AND EPITAXIAL STRAIN

Co grows on Mo(110) in the Nishiyama-Wassermann orientation, i.e., with the hexagonal base plane Co(0001) parallel to Mo(110) and $[\bar{1}100]$Co$\|[\bar{1}10]$Mo.[22,23] Figure 2 shows a superposition of the undistorted bulk planes Mo(110) and Co(0001) in this orientation and Fig. 3 the corresponding electron diffraction patterns. For the description of the film we use a Cartesian system with the *x* axis along [001]Mo, the *y* axis along $[\bar{1}10]$Mo, and the *z* axis along the film normal. Using the lattice parameters $a_{Mo}=0.3147$ nm and $a_{Co}=0.2507$ nm,[31] we obtain along the *x* axis a misfit $f_x=(a_{Co}-a_{Mo})/a_{Mo}=-0.203$ and along the *y* axis a smaller misfit $f_y=(\sqrt{3}a_{Co}-\sqrt{2}a_{Mo})/\sqrt{2}a_{Mo}=-0.024$, both between bulk materials.

For a quantitative analysis of the epitaxial strain, we determined the spot distances b_1, b_2, and b_3 as indicated in Fig. 3 from a series of LEED patterns measured at a fixed electron energy as a function of the sample position, i.e., as a function of the Co thickness of our wedge-shaped sample. The reference values from the Mo(110) substrate, b_1 and $b_{3,Mo}$ were taken from an uncoated area of the Mo(110) sur-

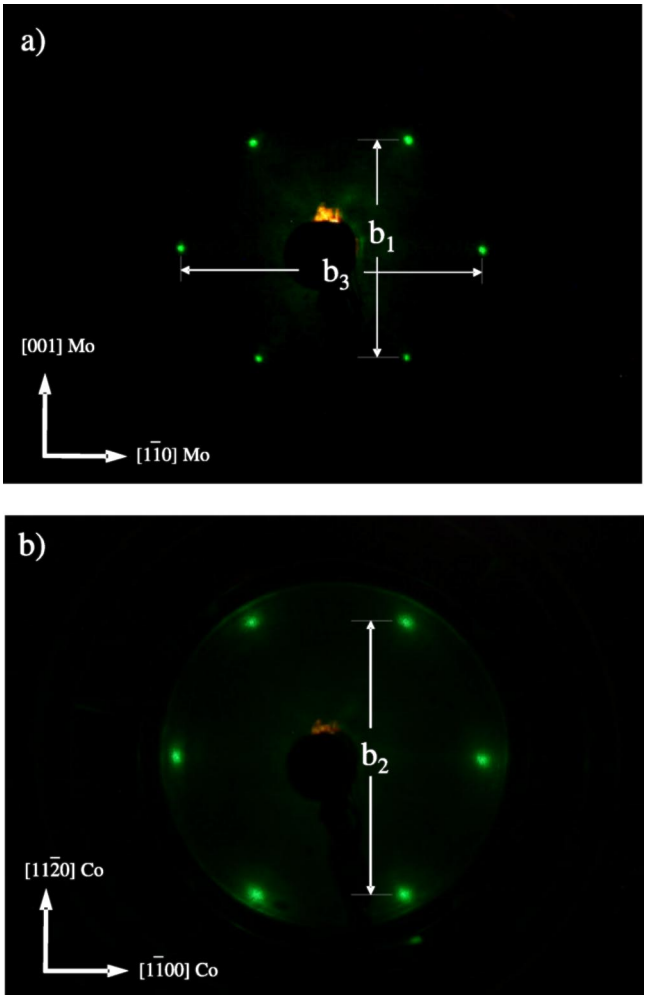

FIG. 3. LEED diffraction patterns of Mo(110) (a) and Co(0001)/Mo(110) (b), incident energy (E_i=65.4 eV).

face. From the ratio b_2/b_1 one calculates the strain $\epsilon_{11}=(a_{\mathrm{Mo}}b_1/a_{\mathrm{Co}}b_2-1)$ along the x axis. The strain along the y axis is determined according to $\epsilon_{22}=(\sqrt{2}a_{\mathrm{Mo}}b_{3,\mathrm{Mo}}/\sqrt{3}a_{\mathrm{Co}}b_3-1)$. Despite very thin film thicknesses below 1 nm, the lateral strains show no dependence on the Co thickness within the error limits (see Fig. 4). Mean values for the lateral strains are $\epsilon_{11}=+0.010\pm0.002$ and $\epsilon_{22}=+0.025\pm0.002$ ($\pm$ signs refer to standard deviation of the mean value, error of individual data are not considered). The value for ϵ_{22} can be explained by pseudomorphic growth along the y axis. From bulk lattice constants one would obtain $\epsilon_{22}=-(\sqrt{3}a_{\mathrm{Co}}-\sqrt{2}a_{\mathrm{Mo}})/\sqrt{3}a_{\mathrm{Co}}=+0.025$ in excellent agreement with the experimental value. The strain along the x axis is slightly larger than the value expected from a locking into a commensurate state with $b_1:b_2=4:5$ that would result in $\epsilon=+0.004$. The expansion of the Co(0001) plane in both directions is in agreement with a previous investigation[22] only for very thin films. For thicker films a compressive strain along the x axis was observed, previously.[22] It cannot be excluded that this discrepancy is due to different growth parameters. The expansion is constant up to a thickness of t=10 nm in contrast to the relaxation observed for the case of Co/W(110) starting at t=2 nm.[12] An increase of the critical thickness for the onset of relaxation for the case of Co/Mo(110) can be expected since the misfit ($f_y=-0.024$) is slightly smaller than in the case of Co/W(110) ($f_y=-0.03$).

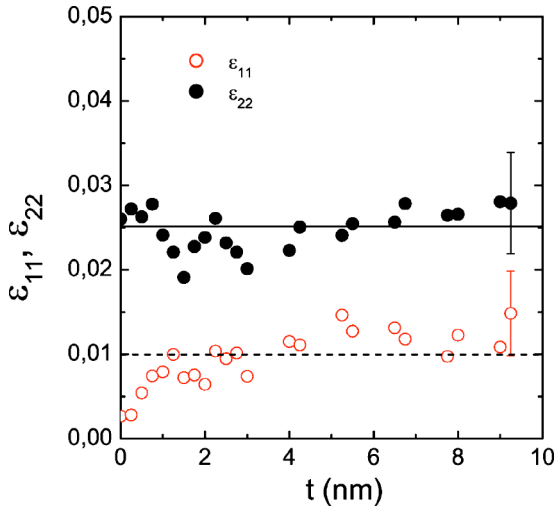

FIG. 4. The latteral strains ϵ_{11} and ϵ_{22} in an epitaxial Co(0001) film on Mo(110) vs thickness t. Mean values for ϵ_{11} and ϵ_{22} are indicated by dashed and full lines, respectively. The error bars for individual data points are depicted only at the last points, for clarity.

IV. MAGNETOMETRY

Magnetization loops as measured with s-polarized light are shown in Fig. 5 for the field applied along the x, y, and z direction. The easy axis loops measured with the field applied along $[1\bar{1}0]$ shows a sudden jump at the coercive field and a residual linear increase at larger fields. The linear increase could be caused by a canted magnetization with an easy axis tilted out of the film plane. However, in this case one would expect a similar linear increase for hard axis loops and a remnant signal for the polar loops both in contrast to the experimental observation. Therefore, we assume that the linear increase is caused by an effective polar Kerr rotation that in turn is due to a small misalignment between external field and the in-plane direction. In the following the linear sections are treated as a linear background signal and subtracted from the Kerr loops.

The polar loops with the field perpendicular to the surface reveal no remnant signal, thus confirming the in-plane easy axis. Saturation can be achieved for all film thicknesses for external fields $\mu_0 H<1$ T. We define an out-of-plane field H_s from the crossing of the initial linear section of the magnetization loop with the saturation signal. For a thickness of t =10 nm the absolute value of the polar Kerr rotation is extremely large (1.5 mrad) compared to the longitudinal Kerr rotation for the same thickness (0.12 mrad).

The evaluation of the in-plane hard-axis loops for the determiation of in-plane MSA is difficult at first sight, since the magnetization loops deviate considerable from the expected reversible behavior. For the evaluation we start from the Kerr rotation $\theta_K^s(H)$ measured with s-polarized light. A similar, nonreversible loop was observed by Osgood *et al.*[24,25] and

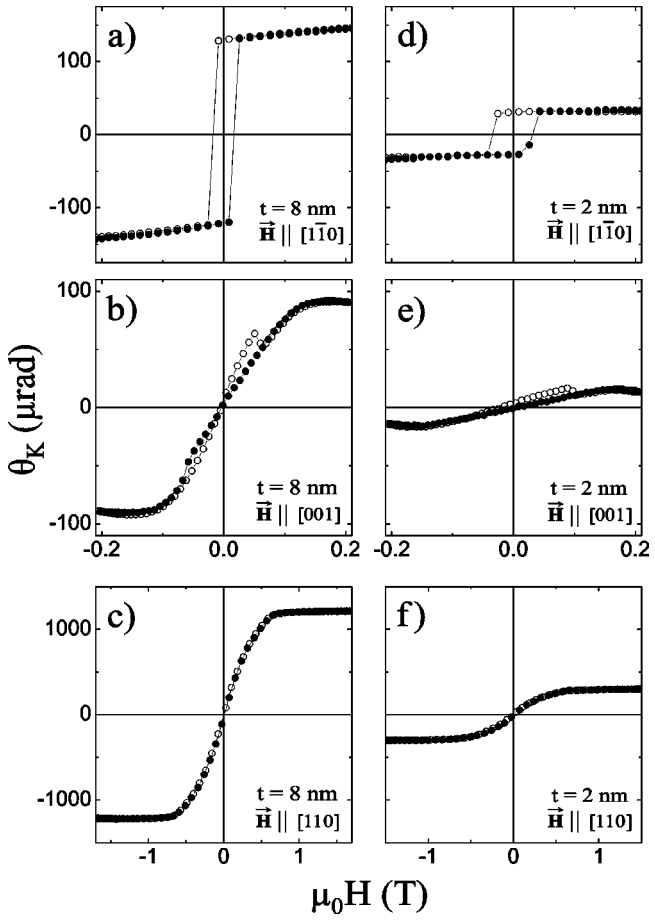

FIG. 5. Magnetization curves as measured with Kerr magnetometry for fields applied along the in-plane easy axis [1$\bar{1}$0]Mo [(a) and (d)], in-plane hard axis [001]Mo [(b) and (e)], and out-of-plane axis [110]Mo [(c) and (f)] for Co/Mo(110) films capped with 3 nm Mo. Co film thicknesses t as indicated in the figure. The Kerr rotation θ_K was measured for s-polarized light.

explained by a nonlinear contribution to the longitudinal Kerr rotation:

$$\theta_K^s = a m_l + b m_l m_t, \tag{1}$$

resulting from the product of the longitudinal and tranversal magnetization components m_l and m_t. In order to extract the longitudinal component, we measured the Kerr rotation with the polarization adjusted between s- and p-polarization (sp) in such a way that $\theta_K^{sp}(-H) = \theta_K^{sp}(+H)$ for H larger than the saturation field [see Fig. 6(b)]. Then $\theta_K^{sp}(H)$ is proportional to the transversal component m_t.[32] We calculate the longitudinal component from the formula

$$m_l(H) \propto \theta_K^s(H) \frac{1}{1 + r\, m_t(H)}, \tag{2}$$

where $r = b/a$ determines the ratio between the regular longitudinal Kerr rotation and the nonlinear term. This ratio is related to the optical constants (see Refs. 24 and 25). We adjust the constant $0.2 < r < 0.3$ such that the irreversible jumps in Fig. 6(c) disappear.

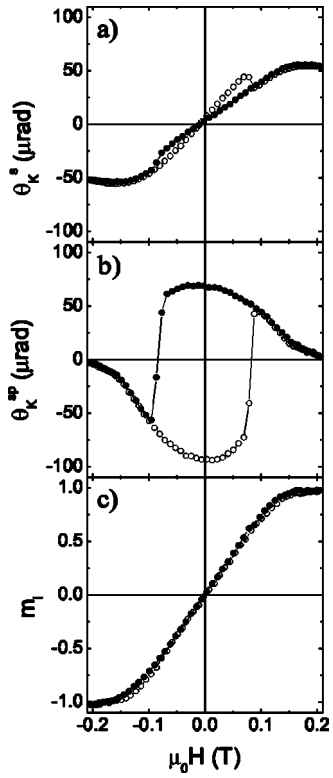

FIG. 6. Longitudinal Kerr rotation $\theta_K^s(H)$ measured with s-polarized light (a) for a 5-nm-thick Co/Mo(110) film capped with 3 nm Mo. The longitudinal Kerr rotation $\theta_K^{sp}(H)$ measured for sp-polarized light (b) is proportional to the transversal magnetization component. The longitudinal magnetization component $m_l(H)$ (c) is obtained using Eq. (2) (see text).

The transversal component m_t shows values with opposite sign for increasing and decreasing field. This indicates that the magnetization reversal process is dominated by a homogeneous (2π) rotation of the magnetization vector rather than by domain wall movement. This behavior is typical for systems with a strong uniaxial anisotropy. The value of the uniaxial anisotropy term is calculated from the anisotropy field H_p determined by the crossing of the initial slope and the saturation value. Data taken from a wedge sample for varying Co thickness are summarized in Fig. 7. For small thicknesses the polar Kerr rotation at saturation $\theta_{K,s}$ follows the relation $\theta_{K,s} = C(t - t_d)$ with an axial section $t_d = (0.1 \pm 0.2)$ nm. If one assumes a proportionality between $\theta_{K,s}$ and the magnetic moment per area, t_d corresponds to a magnetic moment equivalent of $D_d = 0.5$ ML (monolayers). This value can be caused by a change of electronic structure at the interface (surface effect) or by a thermally induced decrease of magnetization (size effect).[10] For Co/W(110) films a similar value of $D_d = 0.9$ ML was determined.[12] For thicker films the Kerr rotation approaches asymptotically a saturation value $[\theta_{K,s} \propto 1 - \exp(-t/t_\lambda)]$ indicating the finite penetration depth $t_{670\ \mathrm{nm}} = (8.8 \pm 0.1)$ nm of the light.

V. EVALUATION OF ANISOTROPIES

We use a fourth order approximation for the volume- and surface-type anisotropy contributions to the free energy

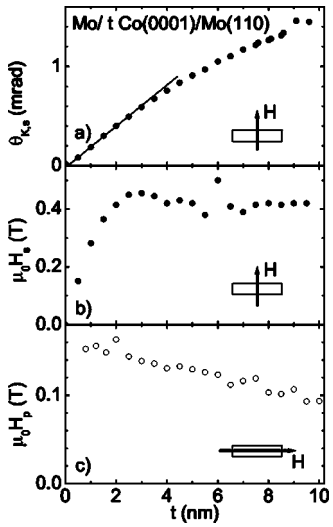

FIG. 7. Saturation value $\theta_{K,s}$ (a) of the polar Kerr rotation and the out-of-plane H_s (b) and in-plane H_p (c) anisotropy fields as a function of the thickness t. Values were taken from a wedge sample 3 nm Mo/0–10 nm Co/Mo(110).

$F(\theta,\phi)$ in order to keep the compatibility to a previous analysis.[33] Using directional cosines $\beta_1=\sin\theta\cos\phi$, $\beta_2=\sin\theta\sin\phi$, and $\beta_3=\cos\theta$ we write for the free energy per volume

$$(1/V)F(\theta,\phi) = (L\beta_3^2 + K_p\beta_1^2) + (K_{4xy}\beta_1^2\beta_2^2 + K_{4yz}\beta_2^2\beta_3^2 + K_{4xz}\beta_1^2\beta_3^2), \tag{3}$$

where the second and fourth order anisotropy constants are composed of volume- and surface-type contributions according to

$$L = J_s^2/2\mu_0 + K_v + (1/t)K_s, \tag{4}$$

$$K_p = K_{v,p} + (1/t)K_{s,p}, \tag{5}$$

and

$$K_{4ik} = K_{v,4ik} + (1/t)K_{s,4ik}. \tag{6}$$

Anisotropy constants are in general obtained from the initial slopes of the hard axis loops that are determined by the second derivatives of the free energy $F_{\theta\theta}(\theta,\phi)$ and $F_{\phi\phi}(\theta,\phi)$ close to the easy axis $\phi,\theta=\pi/2$, given by

$$\frac{1}{A}F_{\theta\theta}\left(\frac{\pi}{2},\frac{\pi}{2}\right) = 2\left[\frac{J_s^2}{2\mu_0} + (K_v + K_{v,4yz})\right]t + 2(K_s + K_{s,4yz}), \tag{7}$$

$$\frac{1}{A}F_{\phi\phi}\left(\frac{\pi}{2},\frac{\pi}{2}\right) = 2(K_{v,p} + K_{v,4xy})t + 2(K_{s,p} + K_{s,4xy}). \tag{8}$$

The second order constants can be separated into different contributions. The out-of-plane and in-plane volume-type anisotropy constants $K_v=K_v^{\rm cr}+K_v^{\rm me}$ and $K_{v,p}=K_{v,p}^{\rm cr}+K_{v,p}^{\rm me}$ are composed of a crystalline contribution $K_v^{\rm cr}$, $K_{v,p}^{\rm cr}$ and a magnetoelastic one $K_v^{\rm me}$, $K_{v,p}^{\rm me}$. The surface-type out-of-plane and in-plane contributions are the sum of a Néel-type and a magnetoelastic anisotropy: $K_s=K_s^{\rm Ne}+K_s^{\rm me}$ and $K_{s,p}=K_{s,p}^{\rm Ne}+K_{s,p}^{\rm me}$, respectively. Additional contributions from the shape anisotropy to the MSA, as discussed in Ref. 12, are neglected here.

We note that for the in-plane anisotropy there is no need for considering fourth order terms since all magnetization loops can be explained by second order anisotropy only. This fact can be directly illustrated by comparing the derivatives of the out-of-plane and the in-plane hard axis magnetization loops, shown in Fig. 8. In general, for the hard axis magnetization loops where contribution of higher order anisotropy terms are negligible, a linear behavior for $M(H)$ and a constant value for dM/dH is expected. Close to saturation, the averaging over a larger area in combination with local defects of the film usually lead to a smearing out of the ex-

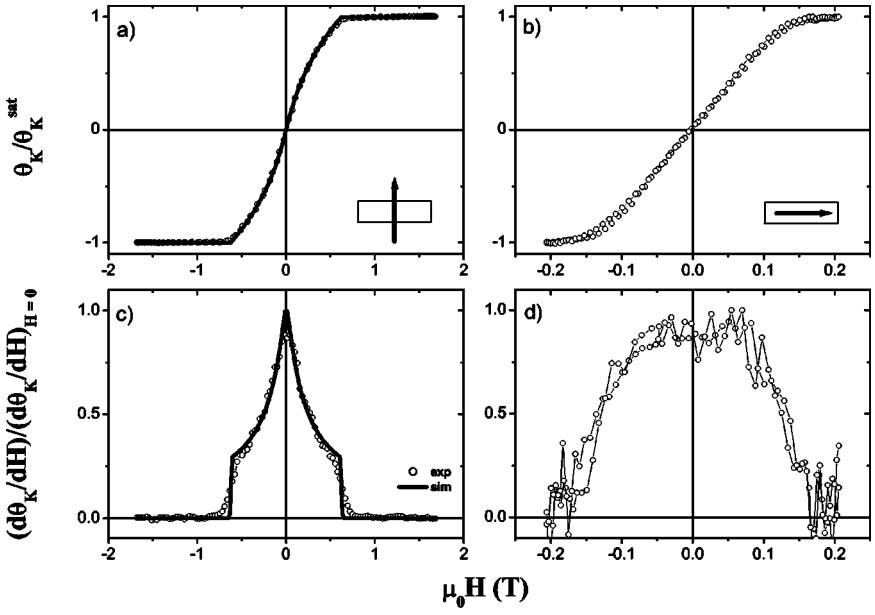

FIG. 8. Examples of hard axis magnetizations loops measured in polar (a) and in longitudinal (b) geometry. The derivatives of the measured loops in (a) and (b) are shown below in (c) and (d), respectively. A comparison of, the simulation of the out-of-plane magnetization curve (a) and its derivative (c), with experiment directly demonstrates the importance of the contribution of the 4th-order terms to the anisotropy for the out-of-plane meas urements.

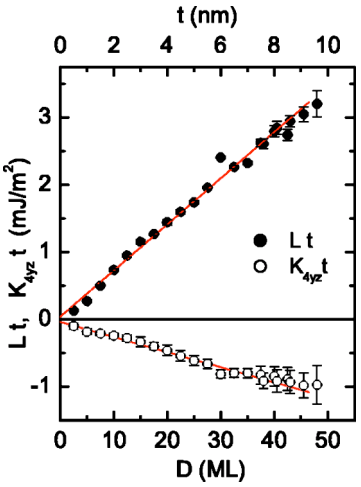

FIG. 9. Out-of-plane anisotropy constants of second order Lt and fourth order $K_{4yz}t$ vs t for Co/Mo(110) capped with Mo. D denotes the thickness in monolayers.

pected kink at saturation. This shows up in Fig. 8(d) as a continuous decrease of the derivative. The derivative of the out-of-plane curve [Fig. 8(c)] qualitatively deviates from this behavior. The derivative shows a step at $\mu_0 H = \pm 0.6$ Tesla that can only be explained by an additional fourth order anisotropy term.

Consequently we fitted the magnetization curves with a model that takes into account second and fourth order anisotropies. From the fit we obtain the anisotropy constants L and K_{4yz} as shown in Fig. 9. Both values Lt and $K_{4yz}t$ describing the total anisotropy per area increase linearly at least for $2 < t < 8$ nm. Systematic deviations to lower anisotropy values are observed for $t < 2$ nm. This fact is more pronounced in the plot of $H_s(t)$ (Fig. 7). It might be attributed to changes of the strain ε_{33} perpendicular to the film plane that could not be measured in this experiment. Values for volume $(K_v, K_{v,4yz})$ and surface $(K_s, K_{s,4yz})$ anisotropies as obtained from linear fits are given in Table I. K_v is obtained from the slope of $L(t)t$ by subtracting the shape anisotropy $J_s^2/2\mu_0$.

TABLE I. Experimental values for in-plane and out-of-plane anisotropy constants for Co films on Mo(110), capped by Mo. Constants are determined for the thickness region $t < 3$ nm. The magnetoelastic constant K_v^{me} is obtained from $K_v = K_v^{me} + K_v^{cr}$ assuming that $K_v^{cr} = -(K_1 + K_2)$ takes on the bulk value of hexagonal-close-packed (hcp) Co. Values obtained from bulk values for crystalline and magnetoelastic constants of hcp Co are given for comparison in the right column.

		Mo/Co(0001)/Mo(110)	bulk hcp Co
$K_{v,p}$	(10^5 J m^{-3})	$+0.79 \pm 0.02$	$+1.2$
K_v	(10^5 J m^{-3})	-9.4 ± 0.1	< -14.8
K_v^{me}		-3.2 ± 0.1	< -7.9
$K_{v,4yz}$		-1.15 ± 0.07	-1.2
$K_{s,p}$	mJ m^{-2}	$+0.04 \pm 0.01$	
K_s	mJ m^{-2}	-0.01 ± 0.01	
$K_{s,4yz}$		-0.03 ± 0.02	

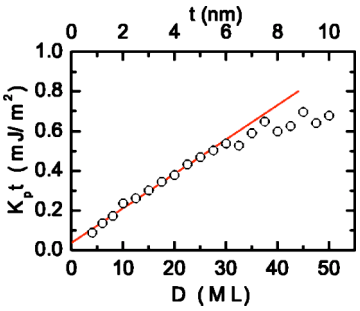

FIG. 10. In-plane anisotropy constant $K_p t$ vs t for Co/Mo(110) capped with Mo. D denotes the thickness in monolayers.

Experimental results for the in-plane anisotropy are obtained from the saturation field H_p. The fourth order constants can be neglected, i.e., $K_{4xy} = 0$, because the in-plane hard axis curves show no significant deviation from a linear increase until saturation is reached [see Figs. 8(b) and 8(d)]. In this case H_p is related to $F_{\phi\phi}(\pi/2, \pi/2)$ according to $H_p = F_{\phi\phi}(\pi/2, \pi/2)/J_s A t = 2K_p/J_s$. We plot $K_p t$ as a function of t (see Fig. 10) in order to separate surface and volume contributions. For $t < 5$ nm $K_p t$ increases linearly with increasing thickness. Values for $K_{v,p}$ and $K_{s,p}$ derived from the slope and the axial section of a linear fit are summarized in Table I. For $t > 5$ nm the anisotropy takes on values smaller than expected from a constant volume contribution. This indicates an onset of strain relaxation that is beyond the accuracy of our structural investigation.

VI. DISCUSSION

Epitaxial strains in our Co/W(110) films persist up to a thickness of 10 nm. This observation is quite surprising because gradual strain relaxation to very small values has been observed for Co/W(110) films with thicknesses larger than 2 nm.[12] For Fe on W(110) and Mo(110) the epitaxial strain relaxes within the first 3–4 monolayers to values less than 1%.[30,34] Because the strain shows no significant thickness dependence between 1 and 10 nm, the magnetoelastic anisotropy contributes only to the volume anisotropy and not to the MSA.

Our experimental values for the MSA are small compared to values reported for many other thin film systems.[10] Particularly small is the out-of-plane interface anisotropy constant K_s for the Mo/Co/Mo(110) system in comparison to the constant reported for Co/W(110) films ($K_s = 0.1$ mJ m^{-2}).[12] Néel-type MSA is attributed to the spin-orbit coupling of magnetic atoms at the interface. The spin-orbit coupling scales with the nuclear charge. Therefore, one might expect a larger MSA for the W than for the Mo interface. However, one should note that contributions to the out-of-plane MSA might originate from magnetoelastic contributions even for constant strain, if the magnetoelastic coupling coefficients at surfaces are different from their bulk values.[14–16,18] Moreover, we neglect the role of thermal excitations on the determination of the MSA from room temperature measurements,[17] which showed up to be important for Ni films. For the case of Co films the Curie temperature

is considerably higher and the temperature effect might be less severe.

The in-plane volume anisotropy $K_{v,p}$ contains no contribution from the crystal anisotropy because of the sixfold in-plane symmetry. $K_{v,p}$ should be of pure magnetoelastic origin, i.e., $K_{v,p}=K_{v,p}^{\mathrm{me}}$. The out-of-plane volume anisotropy $K_v=K_v^{\mathrm{cr}}+K_v^{\mathrm{me}}$ contains crystal and magnetoelastic anisotropy. We extract K_v^{me} by subtracting the bulk value for hcp Co, which is in our notation $K_v^{\mathrm{cr}}=-(K_1+K_2)=-6.2\times10^5$ J m^{-3}. The fourth order constant $K_{v,4yz}$ coincides with the bulk value for hcp Co $K_{v,4yz}=-K_2=-1.2\times10^5$ J m^{-3}. This fact confirms that the film grows mostly hcp and not face-centered-cubic (fcc).

In order to compare the experimental values for magnetoelastic anisotropy contributions we calculate in-plane and out-of-plane magnetoelastic constants according to Refs. 12 and 35:

$$K_v^{\mathrm{me}}=-B_1\epsilon_{22}-B_2\epsilon_{33}-B_3(\epsilon_{11}+\epsilon_{22}), \tag{9}$$

$$K_{v,p}^{\mathrm{me}}=B_1(\epsilon_{11}-\epsilon_{22}). \tag{10}$$

Using magnetostriction constants and elastic constants of bulk hcp Co one obtains $B_1=-0.81\times10^7$ J m^{-3}, $B_2=-2.90\times10^7$ J m^{-3}, and $B_1=+2.82\times10^7$ J m^{-3}. Using the strain values determined in Sec. III we obtain $K_{v,p}^{\mathrm{me}}=+1.2\times10^5$ J m^{-3} in rough agreement with the experimental value. K_v^{me} cannot be determined straightforwardly because we could not determine ϵ_{33}. One would expect a Poisson-type compression resulting from the lateral expansion, i.e., $\epsilon_{33}<0$. Therefore, we can determine a lower limit for the expected size of the magnetoelastic constant: $K_v^{\mathrm{me}}<-7.9\times10^5$ J m^{-3}. The experimental value deviates from this value by more than a factor of 2. Therefore, we conclude that bulk magnetoelasticity does not explain sufficiently well the experimentally observed values, which is not surprising in view of previous work.[14–16,18]

It is interesting to compare the case of Fe films on Mo(110) and W(110). For Fe films the in-plane MSA exhibits a strong uniaxial component on both substrates Mo(110) and W(110) with an opposite sign, although the growth mode for Fe films is similar for Mo(110) and W(110) substrates.[29,30,34,36,37] In both cases the first Fe monolayer grows pseudomorphically and strain-relieving one-dimensional dislocation defects appear in the second Fe layer developing with increasing film thickness into a two-dimensional dislocation network at a coverage of 4 ML. In this way, the epitaxial strain is almost completely relaxed in the first few layers leaving a small constant strain for thicker films.[30,34] Therefore, any contribution from magnetoelastic anisotropy to the MSA in this thickness regime is expected to be small and of similar size and sign for both substrates. The difference is obviously caused by the film/substrate Néel-type interface anisotropy. The determination of MSA for single interfaces[10] reveals that the Fe/W(110) interfaces causes a strong uniaxial component favoring the $[1\bar{1}0]$ in-plane easy axis that overcompensates the second interface of the film in favor of an easy axis along [001]. The Fe/Mo(110) interface causes a much weaker in-plane anisotropy and therefore the easy axis shows in this case along [001].

For the case of Co films on W(110) the film starts to grow mainly hcp(0001)[12,38] with a contribution of fcc(111) oriented areas[39] and in a state of constant strain, with pseudomorphism in the direction $[1\bar{1}00]\mathrm{Co}\|[1\bar{1}0]\mathrm{W}$ (Nishiyama-Wassermann orientation). The constant strain results in this thickness regime in a true volume-type uniaxial magnetoelastic anistropy, favoring an in-plane easy axis along $[1\bar{1}0]$[12] that for all thicknesses wins against the very weak MSA preferring an in-plane easy axis along [001].

In conclusion, the Néel-type interface anisotropies of Fe/W(110) and Co/W(110) interfaces are stronger than the corresponding anisotropies of Fe/Mo(110) and Co/Mo(110) interfaces. We tentatively attribute this fact to the weaker spin-orbit coupling for the lighter element Mo with respect to W.

VII. SUMMARY

We measured magnetic in-plane and out-of-plane anisotropy constants of the system Mo/Co(0001)/Mo(110) grown on α-Al_2O_3. The growth mode of Co on Mo(110) is qualitatively similar to the system Co on W(110). In contrast to the system Co/W(110) the out-of-plane interface anisotropy is very small in this system. This fact may be attributed to the lower nuclear charge providing a smaller spin-orbit coupling of Mo compared to W. The relevant anisotropy contributions can be completely attributed to the epitaxial strain in addition to the crystal anisotropy known from the bulk behavior. Experimental values for the magnetoelastic anisotropy are compared to calculated values using bulk magnetoelastic coupling constants. While the in-plane anisotropy is coincident with bulk magnetostriction behavior, the out-of-plane anisotropy deviates considerably from the expected value. This is not surprising since for Fe films considerable deviations with increasing strain including a change of sign of the magnetostriction constants occurred. The dominance of the magnetoelastic anisotropy in Mo/Co(0001)/Mo(110) films turns this system very interesting for theoretical investigations and comparison to anisotropies of orbital moments.

ACKNOWLEDGMENTS

The authors thank the DFG (Priority Programme 1133 "Ultrafast Magnetization Processes"), the BMBF (Contract No. BMBF 03N6500) and the MWFZ, Mainz, for financial support.

[1] P. Bruno, Phys. Rev. B **39**, 865 (1989).
[2] J. Stöhr and H. König, Phys. Rev. Lett. **75**, 3748 (1995).
[3] H. A. Dürr and G. van der Laan, Phys. Rev. B **54**, R760 (1996).
[4] G. van der Laan, J. Phys.: Condens. Matter **10**, 3239 (1998).
[5] R. Q. Wu and A. J. Freeman, J. Magn. Magn. Mater. **200**, 498 (1999), and references therein.
[6] O. Hjortstam, K. Baberschke, J. M. Wills, B. Johansson, and O. Eriksson, Phys. Rev. B **55**, 15 026 (1996).
[7] L. Néel, J. Phys. Radium **15**, 225 (1954).
[8] R. Koch, M. Weber, K. Thurmer, and K. H. Rieder, J. Magn. Magn. Mater. **159**, L11 (1996).
[9] D. Sander, S. Ouazi, A. Enders, and J. Kirschner, J. Phys.: Condens. Matter **14**, 4165 (2002).
[10] U. Gradmann, in *Handbook of Ferromagnetic Materials*, edited by K. H. J. Buschow (Elsevier, Amsterdam, 1993), Vol. 7, p. 11.
[11] O. Fruchart, J. P. Nozières, and D. Givord, J. Magn. Magn. Mater. **207**, 158 (1999).
[12] H. Fritzsche, J. Kohlhepp, and U. Gradmann, Phys. Rev. B **51**, 15 933 (1995).
[13] T. Gutjahr-Löser, D. Sander, and J. Kirschner, J. Appl. Phys. **87**, 5920 (2000).
[14] D. Sander, Rep. Prog. Phys. **62**, 809 (1999).
[15] M. Farle, Rep. Prog. Phys. **61**, 755 (1998).
[16] O. Song, C. A. Ballentine, and R. C. O'Handley, Appl. Phys. Lett. **64**, 2593 (1994).
[17] K. Baberschke and M. Farle, J. Appl. Phys. **81**, 5038 (1997).
[18] T. Gutjahr-Löser, D. Sander, and J. Kirschner, J. Magn. Magn. Mater. **220**, L1 (2000).
[19] W. Wulfhekel, T. Gutjahr-Löser, F. Zavaliche, D. Sander, and J. Kirschner, Phys. Rev. B **64**, 144422 (2001).
[20] W. A. Jesser and D. Kuhlmann-Wilsdorf, Phys. Status Solidi **19**, 65 (1967).
[21] C. Chappert and P. Bruno, J. Appl. Phys. **64**, 5336 (1988).
[22] M. Tikhov and E. Bauer, Surf. Sci. **232**, 73 (1990).
[23] P. G. Clark, Jr. and C. M. Friend, J. Chem. Phys. **111**, 6991 (1999).
[24] R. M. Osgood III, B. M. Clemens, and R. L. White, Phys. Rev. B **55**, 8990 (1997).
[25] R. M. Osgood III, S. D. Bader, B. M. Clemens, R. L. White, and H. Matsuyama, J. Magn. Magn. Mater. **182**, 297 (1998).
[26] B. M. Clemens, R. M. Osgood III, A. P. Payne, B. M. Lairson, S. Brennan, R. L. White, and W. D. Nix, J. Magn. Magn. Mater. **121**, 37 (1993).
[27] O. Fruchart, S. Jaren, and J. Rothman, Appl. Surf. Sci. **135**, 218 (1998).
[28] U. May, R. Calarco, J. O. Hauch, H. Kittur, M. Fonine, U. Rüdiger, and G. Güntherodt, Surf. Sci. **489**, 144 (2001).
[29] J. Malzbender, M. Przybylski, J. Giergiel, and J. Kirschner, Surf. Sci. **414**, 187 (1998).
[30] S. Murphy, D. Mac Mathuna, G. Mariotto, and I. V. Shvets, Phys. Rev. B **66**, 195417 (2002).
[31] R. W. G. Wyckoff, *Crystal Structures* (Wiley, New York, 1963), Vol. 1, p. 2.
[32] H. Ohldag, N. B. Weber, F. U. Hillebrecht, and E. Kisker, J. Appl. Phys. **91**, 2228 (2002).
[33] H. Fritzsche, H. J. Elmers, and U. Gradmann, J. Magn. Magn. Mater. **135**, 343 (1994).
[34] J. Hauschild, Ph.D. thesis, Technical University of Clausthal, Germany, 1998.
[35] P. Bruno, J. Phys. F: Met. Phys. **18**, 1291 (1988).
[36] U. Gradmann and G. Waller, Surf. Sci. **116**, 539 (1982).
[37] M. Przybylski, I. Kaufmann, and U. Gradmann, Phys. Rev. B **40**, 8631 (1989).
[38] H. Knoppe and E. Bauer, Phys. Rev. B **48**, 1794 (1993).
[39] M. Pratzer and H. J. Elmers, Surf. Sci. **550**, 223 (2004).